# Assessment of the representation of West African storm lifecycles in convection-permitting simulations

Article

Published Version

It is advisable to refer to the publisher's version if you intend to cite from the work.  See [Guidance on citing](Guidance on citing).

# www.reading.ac.uk/centaur

# Assessment of the Representation of West African Storm Lifecycles in Convection-Permitting Simulations

Julia Crook[1] (iD), Cornelia Klein[2] (iD), Sonja Folwell[2] (iD), Christopher M. Taylor[2] (iD), Douglas J. Parker[1] (iD), Rachel Stratton[3] (iD), and Thorwald Stein[4] (iD)

[1]School of Earth and Environment, University of Leeds, Leeds, UK, [2]Centre for Ecology and Hydrology, Wallingford, UK, [3]Met Office, Exeter, UK, [4]University of Reading, Reading, UK

**Abstract** Convection-permitting models perform better at representing the diurnal cycle and the intermittency of convective rainfall over land than parameterized-convection models. However, most of the previous model assessments have been from an Eulerian point of view, while key impacts of the rainfall depend on a storm-relative perspective of the system lifecycle. Here a storm-tracking algorithm is used to generate storm-centered Lagrangian lifecycle statistics of precipitation over West Africa from regional climate model simulations and observations. Two versions of the Met Office Unified Model with and without convection parameterization at 4-, 12-, and 25-km resolution were analyzed. In both of the parameterized-convection simulations, storm lifetimes are too short compared to observations, and storms have no preferred propagation direction; the diurnal cycle of initiations and dissipations and the spatial distribution of storms are also inaccurate. The storms in the convection-permitting simulations have more realistic diurnal cycles and lifetimes but are not as large as the largest observed storms. The convection-permitting model storms propagate in the correct direction, although not as fast as observed storms, and they have a much improved spatial distribution. The rainfall rate of convection-permitting storms is likely too intense compared to observations. The improved representation of the statistics of organized convective lifecycles shows that convection-permitting models provide better simulation of a number of aspects of high-impact weather, which are critical to climate impacts in this important geographic region, providing the high rainfall rates can be taken into account.

## 1. Introduction

Several operational forecast centers have been running their forecast models at high resolution, allowing explicit convection, for a number of years (e.g., Baldauf et al., 2011; Lean et al., 2008). More recently, such models have also been used to make projections of future changes in precipitation with climate change (Ban et al., 2015; Kendon et al., 2017). Low-resolution numerical weather prediction and climate models cannot resolve deep convection explicitly, and their representation of convective precipitation is poor in terms of the diurnal cycle and intermittent nature of rainfall; higher-resolution convection-permitting models tend to represent such precipitation more accurately (Clark et al., 2016; Prein et al., 2015; Weusthoff et al., 2010). Although regional climate models may give a better representation of rainfall than global climate models due to higher resolution and therefore detail of surface type and orography, they still tend to have too much persistent light rain and underestimate the number of dry days and high-intensity events (Kendon et al., 2012), unless a high enough resolution can be achieved to allow the convection parameterization to be switched off. It has been shown that in West Africa the representation of convection (i.e., convection-permitting versus parameterized convection) has a more profound impact on the outgoing longwave radiation (Pearson et al., 2014) and rainfall (Marsham et al., 2013) than the improved resolution. Convection-permitting models also improve the coupling of the rainfall with other parts of the Earth system, notably land surface heterogeneity (Klein et al., 2017; Maurer et al., 2017; Taylor et al., 2013), and as a consequence can bring improvements when used to drive impacts models, such as crop prediction models (Garcia-Carreras et al., 2015).

Almost all of the assessments of convection-permitting models have been from an Eulerian point of view. Assessment of a model's ability to represent convective precipitation is performed by comparing observations and models in a specific storm case study or by various longer-term statistics such as diurnal cycle, daily, monthly, seasonal means, dry spell, and wet spell statistics. However, convective processes

are highly stochastic and in many circumstances it is unreasonable to expect a model to predict rain in exactly the right place at the right time, in which case higher-resolution models may not score well in traditional direct point to point comparisons. For these reasons, alternative evaluation methods have been developed, such as a wavelet approach, fraction skill scores, or comparing characteristics of rainfall objects (Clark et al., 2016, and references therein; Weusthoff et al., 2010).

Although Eulerian evaluation of model rainfall may be technically relatively straightforward, the effect of rainfall in terms of high-impact weather and the feedbacks with other components of the Earth system also depend on the storm lifecycle, in which case a Lagrangian approach (following each storm) is needed. For example, the feedback of convective rainfall with the land surface, while still imperfectly understood, is likely to be different depending on whether a storm is locally initiated or highly organized and propagating into the domain from elsewhere (Hartley et al., 2016). Feedback of storms on the larger-scale circulation also depends on the storm lifecycle through the role of cold pool outflows (Birch et al., 2014, 2013; Garcia-Carreras et al., 2013; Marsham et al., 2013). Numerous studies have produced storm-centered statistics (i.e., from a Lagrangian point of view) for observed storms, for example, using IR imagery over West Africa (Mathon & Laurent, 2001) and over the Americas (Machado et al., 1998), and using combined IR and rainfall radar imagery over Africa and the tropical Atlantic (Futyan & Del Genio, 2007), and over the Sahel (Goyens et al., 2011). Cloud cluster statistics (nontracked) have been produced from microwave satellite imagery over the tropics (Mohr et al., 1999) and sub-SaharanAfrica (Mohr, 2004). Recently, Yang et al. (2017) compared lifetime, event mean precipitation and size distributions of storms tracked using brightness temperature in both a convection-permitting model and in satellite observations over the United States during two summer periods. Reinares Martínez and Chaboureau (2018) compared brightness temperature-tracked storm properties in a convection-permitting simulation and a parameterized-convection simulation with observations over a 6-day period in June over Northern Africa. There are only a limited number of other cases where storm-centered statistics have been used in model-observation comparisons (Caine et al., 2013; Clark et al., 2014; Machado & Chaboureau, 2015; McBeath et al., 2014; Stein et al., 2014, 2015), and these tend to be for a short period and use local radar data.

West Africa is one part of the world where the organization of storms is particularly critical to their dynamic feedbacks and their socioeconomic impact (Parker & Diop-Kane,2017). In the central Sahel, around 90% of the summer rainfall comes from organized, propagating mesoscale convective systems (MCSs), often defined as convective cloud clusters larger than 5,000 $km^2$, while in other parts of the region, isolated and shorter-lived systems provide a greater contribution (Mathon et al., 2002; Mohr et al., 1999). In this study, storm-centered statistics of MCSs over West Africa for the summer months were generated for convection-permitting model simulations, parameterized-convection model simulations, and satellite observations. MCS contributions to rainfall, spatial distribution of different MCS types, storm diurnal cycles, storm development and size, intensity, and propagation speed and direction distributions were compared. In the past, observational studies tracking MCSs used IR satellite products because these were available at a high enough temporal frequency and quality unlike rainfall satellite products, and because cold cloud is usually associated with heavy precipitation. The geostationary nature of IR products makes for robust tracking but does not indicate the position and area of the heavy rainfall or how that moves and develops. With the availability of high temporal resolution quality rainfall products, rainfall tracking becomes a possibility. It is rainfall that has the greater impact on human society; therefore, this paper concentrates on rainfall-tracked storm statistics. The statistics for cold-cloud-tracked storms (presented in the supporting information) were also calculated to compare with previous observational studies and because some future analyses of the simulation data will use the cold-cloud tracking. In many cases the statistics of the two types of tracking show similar results. Two recent versions of the UK Met Office Unified Model were assessed. This model is widely used in both weather forecasting and climate prediction and is being used by a large community of people for climate impact studies, for example, Future Climate For Africa (Stratton et al., 2018), PRIMAVERA (https://www.primavera-h2020.eu/about/), Climate Science for Service Partnership-China (https://www.metoffice.gov.uk/research/collaboration/cssp-china), and Climate Science for Service Partnership-Brazil (https://www.metoffice.gov.uk/research/collaboration/newton/cssp-brazil) projects. The results of this study provide insight on the deficiencies in how the model represents the lifecycle of MCSs and should aid both future model development and the confidence with which we can use model rainfall to drive impacts models for hydrological and agricultural applications. Importantly, many of the

**Table 1**
*Summary of Data Used for Storm Tracking*

| | Time period | Horizontal grid | Temporal resolution | |
|---|---|---|---|---|
| | | | Rainfall | OLR/$T_B$ |
| CMORPH | JJ 2014 JJA 4 years | V_CP12 I_CP4 12 km | 30 min | N/A |
| SEVIRI | JJ 2014 | V_CP12 | N/A | 30 min |
| V_CP4 | JJ 2014 | V_CP12 | 15 min instantaneous | 15 min instantaneous |
| V_CP12 | JJ 2014 | V_CP12 | 15 min instantaneous | 15 min instantaneous |
| V_P12 | JJ 2014 | V_CP12 | 15 min instantaneous | 15 min instantaneous |
| I_CP4 | JJA 4 years | I_CP4 12 km | 15-min mean | hourly mean |
| I_P25 | JJA 4 years | I_P25 | hourly mean | hourly mean |

differences in Eulerian statistics of precipitation between convection-permitting and parameterized-convection configurations are generic across models (Prein et al., 2015). Therefore, conclusions from this study are likely to be applicable to other models. Section 2 describes the models and observations used, section 3 describes the storm tracking algorithm applied, and section 4 presents the results. A summary of the findings and the key conclusions are presented in section 5.

## 2. Models and Observations

A storm-tracking algorithm (section 3) was employed to identify and track storms based on rainfall outputs from model simulations and satellite rainfall observations. Tracking was also performed on top of atmosphere outgoing longwave radiation (OLR) outputs from model simulations and satellite infrared brightness temperatures ($T_B$). This section describes the two different UK Met Office models and their simulations and the satellite data sets used. Note that high temporal resolution data (<= hourly) are required to perform storm tracking of MCS so that a storm does not move too much between time steps and therefore the clusters in consecutive images that are part of the same storm overlap sufficiently for the tracking algorithm to recognize such clusters to be the same storm. Ideally, all data should be on the same horizontal grid and at the same temporal resolution for the best comparison so that differences can be attributed to the model's ability to represent convection rather than differences in spatial or temporal resolution used for tracking. Different spatial and temporal resolution will clearly give different rainfall intensity distributions. Where possible, data were regridded to a consistent horizontal grid. The simulation and satellite data used for tracking are summarized in Table 1.

### 2.1. Models

Within the Vegetation Effects on Rainfall in West Africa (VERA) project, simulations using the UK Met Office atmosphere-only Unified Model (UM v8.2) were run for a single season (April through July 2014) over the West Africa domain (approximately 20°W–20°E,0°N–25°N) at 4- and 12-km resolutions. The model uses a semi-implicit, semi-Lagrangian numerical nonhydrostatic, deep atmosphere dynamics scheme (Davies et al., 2005) and includes a comprehensive set of parameterizations describing the land surface (JULES; Best et al., 2011; Clark et al., 2011), boundary layer (Lock et al., 2000), convection (Gregory & Rowntree, 1990) with closure based on the convective available potential energy, and cloud microphysics (Wilson & Ballard, 1999). The model has 70 model levels, which equates to an 80 km top for 12-km resolution and 40 km top for 4-km resolution. The soil properties were set to sandy soil type over the whole domain and the bare soil emissivity set to 0.9, closely matching observations in this region (Ogawa & Schmugge, 2004; Vogel et al., 2011; Zhou et al., 2011). The vegetation fractions were set to current vegetation based on the European Space Agency CCI land cover data set v1.4 for the 2008–2012 epoch (Poulter et al., 2015). Sea surface temperatures and boundary conditions were prescribed from ERA-Interim data (Dee et al., 2011) every 6 hr. The initial soil moisture climatology was determined by running the land surface model JULES offline, forced with the WATCH Forcing Data-ERA-Interim data (Weedon et al., 2014) for 1979–2014 and with the current vegetation fractions, and producing a climatology from the 2000–2014 output. Simulations were performed at 12-km resolution using the parameterized convection scheme (hereafter referred to as V_P12); another 12-km simulation (hereafter referred to as V_CP12) and a 4-km simulation (hereafter referred to as V_CP4) were run with the parameterization scheme switched on but severely restricting its effect by adjusting the relaxation time, and subgrid 3-D Smagorinsky-type mixing employed, allowing explicit convection. The only difference between V_CP12 and V_P12 is therefore the convection parameterization. In these simulations, tracking was performed on instantaneous rain rate and OLR, output at 15-min intervals. Statistics were produced for June and July having first regridded the 4-km data to the V_CP12 grid before storm tracking was performed. Although these simulations are for only one season, all simulation data used for tracking were at the same temporal and spatial resolution, making the statistics easier to compare.

Within the Future Climate For Africa Improving Model Processes for African cLimAte project, simulations using the UM Met Office regional model (v10.3) were run for 10 current climate years over the whole of

Africa at 4.5- and 25-km resolutions. The simulations are described in detail in Stratton et al. (2018). At the time of analysis 5 years of current data were available. The ~4.5-km convection-permitting simulation is hereafter referred to as I_CP4. The ~25-km regional model is hereafter referred to as I_P25. Soil properties were set to sandy soil type across the domain for I_CP4, but by mistake the I_P25 simulation was left with the standard UM soil-type configuration. This affects a number of soil properties. Maps of these properties for the standard UM soil and for sandy soil are shown in supporting information Figure S1. Vegetation fractions were very similar to that used for VERA simulations. The I_CP4 simulations output 15-min mean rain rate and hourly mean OLR; the I_P25 simulations output hourly mean rain rate and OLR. I_CP4 data were regridded to an ~12-km grid before storm tracking was performed, but for I_P25 the tracking was performed on the ~25-km grid. Statistics for four different years (June, July, and August) between 1997 and 2004 were produced, providing a better climatology than the single season for the VERA simulations. However, when comparing statistics of storms, the different spatial and temporal resolutions of the data used for tracking must be taken into account and differences between convection-permitting and parameterized-convection simulations may not be just due to the convection parameterization.

### 2.2. Observations

For comparison with simulated rainfall the bias-corrected CMORPH 8-km30-min data set (Xie et al., 2017) was used. This product combines low-orbiting satellite passive microwave observations with geostationary satellite infrared observations to track precipitation features and fill in the gaps when the microwave observations are not available (Joyce et al., 2004). If a precipitation feature is visible in one passive microwave sensor scan but not in the next available passive microwave sensor scan, the geostationary data cannot be used to interpolate the precipitation associated with that feature beyond the last time the feature was seen in the passive microwave sensor scan. This means storm lifetimes may be found to be lower than they truly are. This will affect the timing of initiations and dissipations to some extent and the timing of when maximum size and intensity are reached. The raw CMORPH data are also bias corrected through probability density function matching against the Climate Prediction Center (CPC) daily gauge analysis over land. Due to the lack of long-term ground station data over Africa, it is difficult to assess the accuracy of CMORPH in this region. However, Berthou et al. (2019) show that although CMORPH has generally slightly lower 3-hourly rain rates on a 0.25° grid than the commonly used TRMM 3B42RT product in this region during the monsoon season, and is particularly low over the Guinea Highlands, CMORPH rain rate distributions compare well with AMMA-CATCH rain gauge 3-hourly data sets in Mali, Niger, and Benin. Four years of data for June, July, and August between 2002 and 2006 were regridded to the I_CP4 12-km grid before tracking was performed. June and July 2014 data were regridded to the V_CP12 grid before storm tracking was performed.

The Tropical Rainfall Measuring Mission (TRMM) radar product 2A25 (NASA, https://pmm.nasa.gov/) for June and July 2004–2014 was used to compare rainfall cluster statistics but cannot be used for tracking. TRMM has two to four overpasses a day over West Africa at ~5-km resolution, providing more accurate (no gap filling), albeit infrequent 247-km-wide snapshots of varying north-south extent. Although the correction algorithms employed have been improved in the most recent version of this product, it is likely that rain rates >10 mm/hr are still underestimated (Kirtsetter et al., 2013).

The Meteosat Second Generation (10.8-μm channel) SEVIRI brightness temperature ($T_B$; Schmetz et al., 2002) at 30-min time resolution and 5-km spatial resolution was used to compare with the storm tracking from modeled OLR. To convert modeled OLR to a brightness temperature for comparison with SEVIRI, the Stefan Boltzmann equation was used:

$$OLR = \sigma T_B{}^4 \tag{1}$$

SEVIRI data for June and July 2014 were regridded to the V_CP12 grid before storm tracking was performed. The advantage of using SEVIRI data is that it is ideal for tracking because it is subhourly geostationary data.

## 3. Storm Tracking

A storm-tracking algorithm (Stein et al., 2014) was employed to identify storms based on rainfall or OLR/$T_B$, which are tracked in time using an area overlap criterion. At each time step, clusters are identified as contiguous grid cells meeting a certain threshold. For rainfall a threshold of >1 mm/hr was used; for
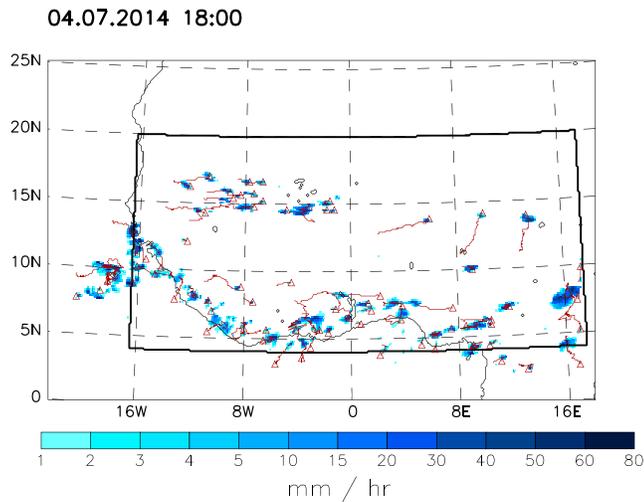
**Figure 1.** A snapshot of thresholded rainfall rate from the V_CP12 simulation with the tracks of MCS storms existing at that time. Magenta triangles show the initiation points, magenta lines show the tracks for times before and after this snapshot, and blue shading shows the thresholded rainfall rate. The black box outlines the area in which MCS were analyzed over land for the statistics.

modeled OLR a threshold of <167 W/m$^2$, equivalent to a SEVIRI $T_B$ of <233 K (−40 °C) using equation (1), was used. These are commonly adopted thresholds for identifying storms in West Africa (Goyens et al., 2011; Taylor et al., 2013). Here the term cluster is defined as contiguous grid cells that meet the threshold at a particular time step, whereas a storm is defined as clusters that propagate over a number of time steps and therefore have a lifecycle from initiation to dissipation. A cluster may be a single grid cell. Between consecutive images, clusters may propagate. A velocity field calculated by cross correlation of images at time $t_i$ and $t_{i-1}$ is used to advect the clusters at time $t_{i-1}$ before areal overlap with the clusters at time $t_i$ is determined. A cluster at time $t_i$ is deemed to be the same storm as a cluster at time $t_{i-1}$ if the fractional overlap of the clusters is greater than 0.6. When a cluster at time $t_i$ does not overlap with any preexisting clusters, it is considered to be a newly initiated storm. When a cluster (named as storm X) at time $t_{i-1}$ does not overlap with any clusters at time $t_i$, storm X ceases to exist and is said to have dissipated. If more than one cluster at time $t_i$ overlaps sufficiently with one cluster (named as storm X) at time $t_{i-1}$, the cluster with the largest overlap keeps the storm ID X, while the other clusters are said to have split off from storm X forming new storms (split initiations). When a cluster at time $t_i$ overlaps sufficiently with more than one cluster at time $t_{i-1}$, the storms identified by these clusters at time $t_{i-1}$ are defined as mergers. The cluster at time $t_i$ takes the storm ID of the cluster at time $t_{i-1}$ with the largest overlap. At each time step the storm-tracking algorithm saves for each storm the area of the cluster, the minimum, mean, and maximum rain rate or OLR/$T_B$ over the cluster, the center point of the cluster and the location of the box outlining the cluster.

Hereafter, an MCS is defined as a storm that reaches a size of at least 1,000 km$^2$ for rainfall and at least 5,000 km$^2$ for OLR/$T_B$ at some point in its lifetime. These are commonly adopted size definitions (Goyens et al., 2011; Taylor et al., 2013). Rainfall clusters are generally smaller than cold cloud clusters, and under a cold cloud cluster there is likely to be more than one rainfall cluster. Therefore, the size definitions for MCS are different for rainfall and cold cloud. The statistics presented are for MCSs over the land within the region 16.5 W–17.5°E, 4.0°N–20.0°N. Figure 1 shows the domain used and example storm tracks from tracking of rainfall from the V_CP12 simulation. The equivalent plot for tracking of OLR is in supporting information Figure S2. Using the given thresholds for rainfall tracking, about 80% of the rainfall MCSs for both CMORPH and V_CP12 had associated cold cloud and therefore this definition of a rainfall MCS is largely consistent with that of a cold cloud MCS.

## 4. Results

### 4.1. Number of Storms/Clusters

In this section, the model simulations are assessed for how well they produce the correct number of storms, proportion of MCSs, and the contribution of MCS rainfall to the total rainfall.

Although the percentage of CMORPH storms that reach MCS size at some point during their life cycle is 22%, MCS-sized CMORPH clusters make up 40% of all cluster occurrences due to MCSs living longer than small storms (Table 2) and contribute more than 90% to total rainfall, underlining the importance of MCSs in this region. It has previously been shown that MCSs account for ~90% of the rainfall in the central Sahel (Mathon et al., 2002) and ~78% in sub-SaharanAfrica (Mohr et al., 1999). The V_P12 simulation has the worst performance with almost 30 times more storms than CMORPH. Due to a large number of small storms, V_P12 exhibits a lower percentage of MCS-sized storms and clusters, although the total number of MCSs exceeds that of all other simulations. The I_P25 simulation is the only simulation at 25 km, a resolution at which only two contiguous grid cells is required to meet the MCS criterion (12-km data require seven). Therefore, small storms cannot be resolved and the percentage of MCS storms is much greater than for any other simulation. Convection-permitting simulations (V_CP4, V_CP12, and I_CP4) overestimate the number of storms but show a proportion of MCS-sized clusters and storms

**Table 2**
*Numbers and Percentages of Storms and Clusters Over Land Based On Rainfall*

| | Storm statistics | | Cluster statistics | | Seasonal mean rainfall accumulation (mm) |
|---|---|---|---|---|---|
| | Number of storms per month | Number of storms that reach MCS size per month (%) | Percentage of clusters > MCS size(%) | Percentage of accumulated rainfall from clusters > MCS size(%) | |
| CMORPH | 12,715 | 2,858 (22%) | 40 | 96 | 167 (JJ) 323 (JJA) |
| V_CP4 | 39,966 | 5,430 (14%) | 27 | 91 | 297 |
| V_CP12 | 15,455 | 3,652 (24%) | 46 | 97 | 368 |
| V_P12 | 366,277 | 35,649 (10%) | 10 | 54 | 210 |
| I_CP4 | 46,680 | 6,539 (14%) | 20 | 70 | 442 |
| I_P25 | 13,065 | 10,789 (83%) | 85 | 99 | 376 |

considerably closer to CMORPH than V_P12. Interestingly, both these measures are best captured by V_CP12 in spite of the low resolution, which allows only a coarse representation of convective circulation. The total number of storms is dependent on the resolution of the data (e.g., comparing tracking at 4 km with tracking after regridding to 12 km) but the number of MCSs is very similar. Therefore, this study concentrates on statistics of MCS.

The contribution to total rainfall accumulation from MCS is similar to CMORPH in percentage terms for V_CP4 and V_CP12, although the seasonal mean total accumulations for these simulations are considerably higher (1.8 and 2.2 × higher) than for CMORPH. The V_P12 simulation has a relatively low percentage MCS contribution (54%) to rainfall, although the seasonal mean total accumulation is slightly higher (1.26 ×) than CMORPH. The I_CP4 simulation also has a notably lower contribution to total rainfall from MCSs than observations and other convection-permitting simulations, although it has a higher (1.4 ×) seasonal mean total accumulation than CMORPH.

### 4.2. Diurnal Cycle and Lifetime

The time of day at which rainfall peaks does not affect daily means but does affect the feedbacks on the energy balance and water cycle (Birch et al., 2014; Marsham et al., 2013). In this section the simulations are assessed for their ability to initiate and dissipate storms at the correct time of day. The difference between dissipation time and initiation time gives the lifetime of a storm. Note that storms may initiate by splitting off another storm or by being spontaneously generated and may dissipate by merging into another storm or by spontaneously disappearing. In line with many previous studies (e.g., Marsham et al., 2013), parameterized-convection simulations (V_P12 and I_P25) exhibit a different rainfall-tracked storm diurnal cycle for MCSs over land to convection-permitting simulations (V_CP4, V_CP12, and I_CP4) and observations, with initiations and dissipations happening earlier in the day (Figures 2a and 2b). CMORPH initiations occur over a much broader time period than simulated initiations but peak at 16:00. V_CP4 and V_CP12 initiations also peak at 16:00, whereas V_P12 initiations peak at 14:00. The I_CP4 initiations peak at 15:00; this peak is at the same time as I_P25 initiations, but the curve is mostly shifted later in the day for I_CP4 by about 1 hr compared to I_P25.

An important failing of many models with parametrized convection is the inability to maintain nocturnal deep convection over land. In Figure 2a it can be seen that V_P12 has too few storm initiations overnight relative to CMORPH, while all the other simulations, including the convection-permitting simulations and I_P25, have frequencies of initiation much closer to CMORPH. Given the number of differences between I_P25 and V_P12, including completely different dynamics, it is difficult to explain what causes I_P25 to behave better.

The differences in dissipation times (Figure 2b) between parameterized-convection and convection-permitting simulations are greater than the differences in initiation times. I_CP4 dissipations peak at 18:00, V_CP4 and CMORPH dissipations peak at 20:00, and V_CP12 dissipations peak at 22:00; the parameterized-convection simulations (V_P12 and I_P25) peak much earlier at 15:00–16:00, consistent with many of the storms initiated during the day being very short-lived. In V_P12 and I_P25 there are many fewer
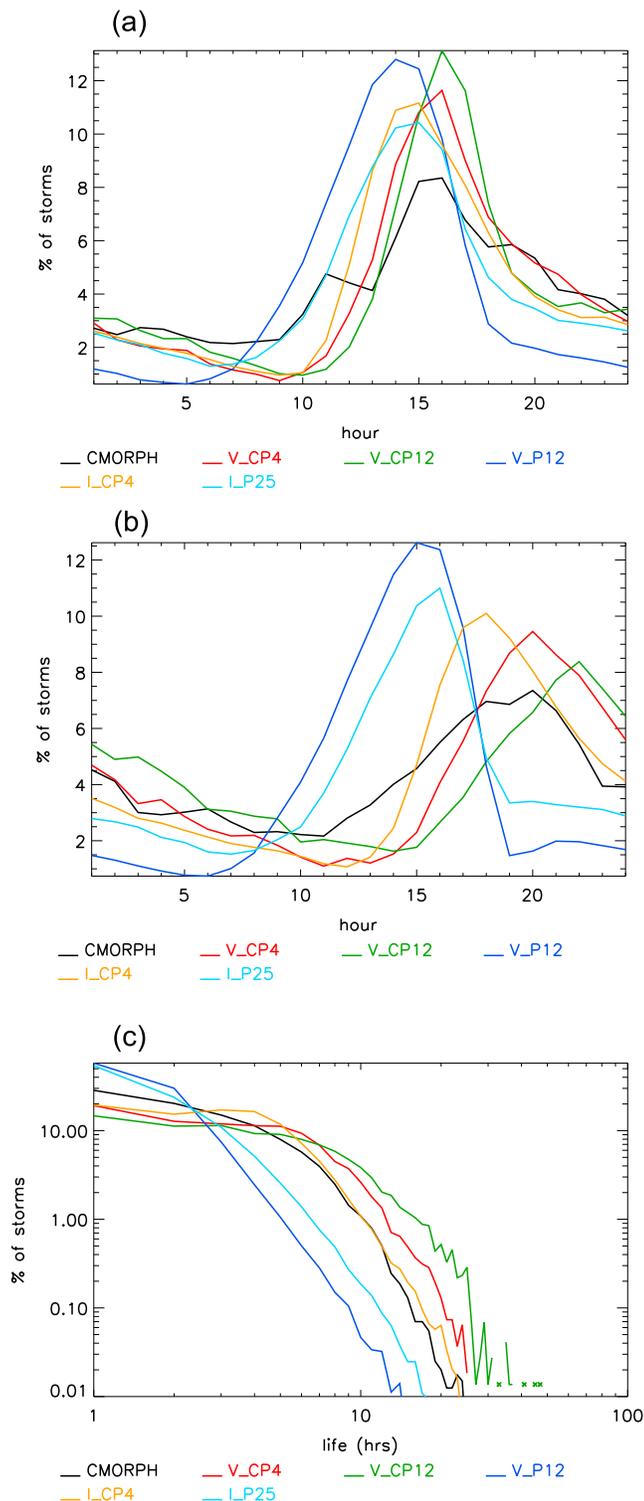
**Figure 2.** Diurnal cycle of (a) initiations and (b) dissipations to the nearest hour of the day (UTC) for MCS over land. (c) Lifetime distributions, binned in hourly bins for MCS over land. Points marked with an x show values that could not be drawn with a continuous line because adjacent bins have values that fall below 0.01%.

dissipations in the evening and overnight compared to CMORPH and other simulations, showing that convection does not persist into the night for parameterized-convection models but does for convection-permitting models. The stochastic perturbations added in the boundary layer in I_CP4 enhance the triggering of convection (Stratton et al., 2018) and will affect the timing of initiations. This may be the reason I_CP4 initiations/dissipations occur earlier than V_CP4 and V_CP12 initiations/dissipations.

The resolution of diagnostics may influence the initiation and dissipation distributions of Figure 2. The tracking of I_P25 precipitation was at 25 km and hourly resolution, whereas other simulations were tracked at 12-km and 15-min resolution. At a lower spatial resolution, where mean rainfall rates over a grid box are often smaller, one might expect that a storm would not be detected so soon after true initiation and would no longer be detectable sooner than true dissipation time; that is, measured initiation time would be later and measured dissipation time would be earlier than at higher resolution. It is less clear what the impact of lower time resolution would be. However, a comparison of initiation times, dissipation times, and lifetimes from tracking of hourly means compared to 15 min means showed little difference in I_CP4 (not shown).

MCSs in parameterized-convection simulations (V_P12 and I_P25) have shorter lifetimes (Figure 2c) than those in convection-permitting simulations (V_CP4, V_CP12, and I_CP4) and observations. In V_P12 and I_P25 the number of storms drops off very rapidly for lifetimes >2 hr and it is very rare (<~0.2%) for a storm to live more than 10 hr. In V_CP4, V_CP12, I_CP4, and CMORPH a significant number of storms (>2%) can live for 10 hr. Lifetimes can occasionally reach 20 hr for I_CP4 and CMORPH, 25 hr for V_CP4, and ~40 hr for V_CP12.

The diurnal cycle of storms as measured by OLR/$T_B$ also shows initiations and dissipations happening earlier in the day for parameterized-convection simulations than convection-permitting simulations, (supporting information Figures S3a and S3b). The diurnal cycle of initiations and dissipations for SEVIRI (peaking at 16:00 and 21:00, respectively) is very similar to that found by Mathon and Laurent (2001) from an 8-year climatology of $T_B$ over the Sahel. Lifetimes measured with SEVIRI and CMORPH are similar, likely due to the fact that the CMORPH product uses SEVIRI data to fill in the gaps in time and space when the microwave data are not available, although SEVIRI displays a slight peak at 2–3 hr and has a higher percentage of storms with lifetimes in excess of 10 hr suggesting the cold cloud of an MCS may outlive its rainfall. They are also very similar to the Sahelian lifetime distributions measured by Mathon and Laurent (2001), although they found around 0.01% of storms had lifetimes of about 60 hr from an 8-year climatology of $T_B$. Yang et al. (2017) also found that storms in their convection-permitting model had slightly longer lifetimes than in observations over the United States. Reinarez Martínez and Chaboureau (2018) also found improvements in the diurnal cycle of brightness-temperature-tracked storms over West Africa in their convection-permitting simulation compared to their parametrized-convection simulation despite their short analysis period.

In summary, convection-permitting simulations show an improvement in diurnal cycles compared to parameterized-convection simulations with initiation and dissipations happening later in the day in convection-
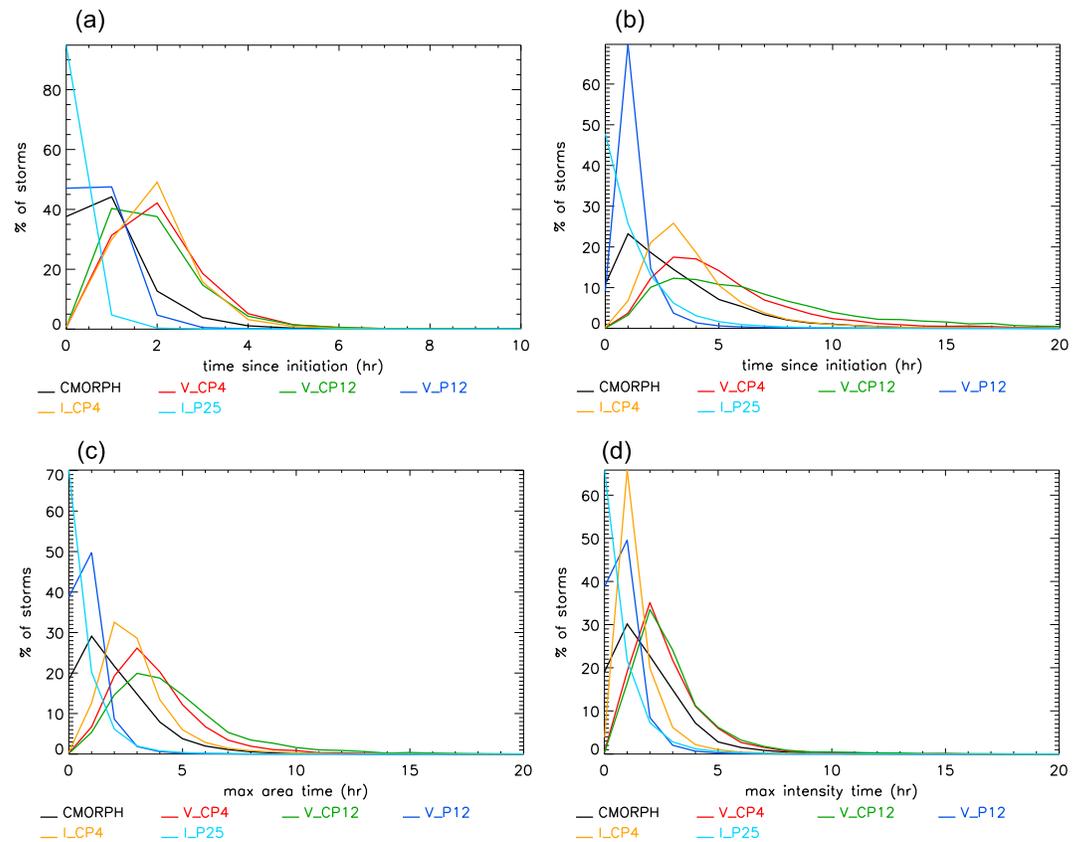
**Figure 3.** Distributions of time since initiation when (a) spontaneously initiated storms reached MCS size, (b) spontaneously initiated storms were no longer of MCS size, (c) spontaneously initiated storms reached maximum size, and (d) spontaneously initiated storms reached maximum cluster-mean intensity.

permitting simulations. Parameterized-convection lifetimes are too short compared to observations and convection-permitting simulations have improved lifetimes, but the V_CP12 simulation lifetimes were up to ~15 hr too long.

### 4.3. Development of MCSs

In this section, simulations are assessed for how MCS storms develop over their lifetime compared to observed MCSs. Figure 3a shows the time since initiation when spontaneously initiated MCSs first reach MCS size. Note that one might expect that split-initiated storms would be largest near the beginning of their life and then decay unlike spontaneously initiated storms, so those are not included here. For CMORPH the peak in this time occurs at 1 hr but 5% of the MCSs take at least 3 hr. For convection-permitting simulations (V_CP4, V_CP12, and I_CP4) storms take longer to reach MCS size than CMORPH (peaking at 1–2 hr and with ~5% taking 4 hr). For V_P12 the behavior is more similar to CMORPH, although times are slightly shorter. I_P25 storms reach MCS size more quickly than CMORPH. This is partly due to the lower resolution of I_P25 where only two grid cells are needed to reach MCS size.

The peak in the time at which spontaneously initiated MCS storms become smaller than MCS size occurs at 1 hr for CMORPH but a significant number (>5%) take 7–8 hr; Figure 3b). This time is slightly longer for convection-permitting simulations (V_CP4, V_CP12, and I_CP4), where percentages of storms peak at 3–4 hr and decay at a similar rate to CMORPH. The percentage of storms decays rapidly for V_P12 and I_P25 after 1 hr.

Figure 3c shows the time since initiation to reach maximum area for spontaneously initiated MCSs. The maximum area is reached very quickly for V_P12 and I_P25 (peak within 1 hr and decaying to 5% by 2–3 hr). For CMORPH the peak is also at 1 hr but about 5% of the MCSs take 6 hr to reach maximum size.

For convection-permitting simulations (V_CP4, V_CP12, and I_CP4), the peak is at 2–4 hr with ~5% taking up to about 8 hr. I_CP4 most closely matches CMORPH.

The time since initiation when the maximum intensity (maximum of cluster-mean rain rate over lifetime) is reached for spontaneously initiated MCS storms (Figure 3d) peaks in the first hour in V_P12, peaks immediately in I_P25, and drops off rapidly within the first 3 hr for both V_P12 and I_P25. For CMORPH the peak is also in the first hour but a significant number of storms (~4%) take 6 hr. For V_CP4 and V_CP12 the peak is at 2 hr with a significant number (>2%) taking 8 hr. I_CP4 peaks in the first hour but has a narrower band of maximum intensity times than CMORPH.

Differences between all simulations and CMORPH are partly due to the different time resolution of the tracking. When tracked at 15 min, I_CP4 has no storms that initiate at MCS or maximum size or maximum intensity, whereas when tracked hourly, between 20%–30% of storms initiate at MCS or maximum size and maximum intensity and the histograms are shifted to the left by about an hour (not shown). All the MCS size development histograms for hourly tracking of I_CP4 are much closer to those for CMORPH than I_CP4 tracked at 15 min. V_P12 is also tracked at 15-min resolution yet does have around 40% of storms initiating at MCS or maximum size and maximum intensity showing that storms in parameterized-convection simulations do develop more quickly than in convection-permitting simulations. It is possible that some storms in CMORPH are not seen when they first exist due to microwave scans not being available at that time (see section 2.2). It is also possible that because intensities in CMORPH are generally a bit lower than in convection-permitting simulations, when a storm first initiates, its intensity is below the threshold and so is not seen in the tracking algorithm making development times shorter. However, storm development time distributions for storms tracked using OLR/$T_B$ (supporting information Figure S4) are very similar for SEVIRI and CMORPH and there are similar differences between simulations and observations. The time to reach minimum $T_B$ for SEVIRI is shorter than the time to reach maximum rain rate for CMORPH; this is most clearly seen in the tail of the distributions.

In summary, due to the different time resolution of the simulations and observations, it is difficult to reach firm conclusions about which simulations better represent observed MCS development times in terms of size and intensity, although it is likely that storms in parameterized-convection simulations develop too quickly and the tails of the distributions are too short. MCSs develop in terms of size and intensity more slowly in convection-permitting simulations than in parameterized-convection simulations.

### 4.4. Size

In this section simulations are assessed for how well they represent the distribution of storm sizes. Both the mean storm equivalent radius and the cluster area distributions for MCS storms (Figures 4a and 4c) show that CMORPH has storms that become considerably larger than all simulations except for I_P25. The maximum storm area distributions (Figure 4b) present similar behavior, although V_CP12 performs better, suggesting that V_CP12 storms may reach large sizes but do not stay very large for as long as observed storms. The peak in the mean radius for CMORPH occurs at ~20 km, is slightly less (~13–16 km) for V_CP4, V_CP12, V_P12, and I_CP4, but with the V_P12 curve shifted the most to smaller radii. Due to the lower resolution of I_P25, the smallest clusters are not seen and therefore the distribution is shifted to larger sizes. Under synoptic control the parameterized convection can cause precipitation in lots of grid cells independently so that, although the storms are not organized as they are in convection-permitting simulations, contiguous areas of precipitating grid cells can still be large. Area distributions based on clusters (Figures 4c and 4d) also includes data from the TRMM radar, which is in good agreement with CMORPH. One would not necessarily expect the TRMM radar to show such big storms as CMORPH because the radar has a swath width of 247 km and for some storms the full E-W width may not be seen. However, as shown in Figure 4 a, the CMORPH mean equivalent radius is usually below 100 km. Figure 4d suggests that a larger percentage of the rainfall comes from very large storms in both CMORPH and TRMM radar than all simulations except I_P25. When tracking with OLR/$T_B$, size distributions are more similar between simulations and observations (supporting information Figure S5), although V_P12 still has the smallest peak mean effective radius and storm clusters can reach much larger areas for observations than in any simulation except I_P25. Yang et al. (2017) also found that their convection-permitting model underestimated storm areas compared to observations over the United States and Reinarez Martínez and Chaboureau (2018) also found improvements in the size of brightness-temperature-tracked storms over West Africa in their convection-permitting
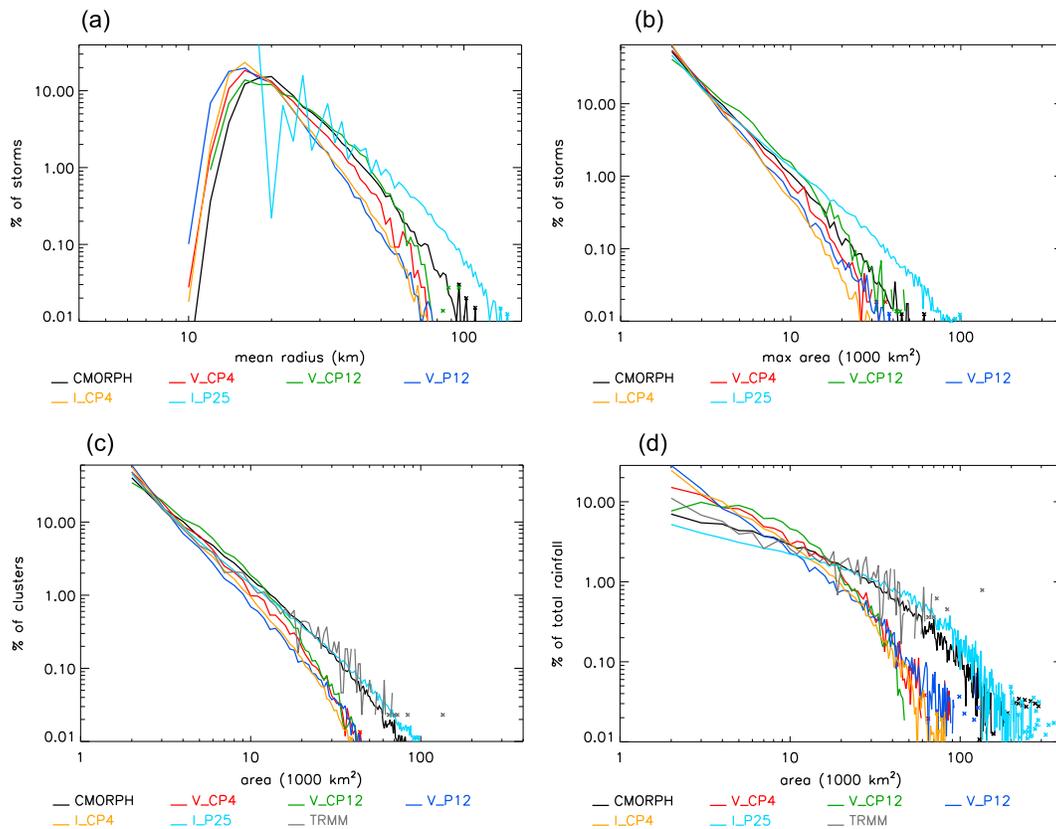
**Figure 4.** (a) Mean equivalent storm radius distributions binned every 2 km, (b) maximum storm area distributions binned every 1,000 km$^2$, and area distributions binned every 1,000 km$^2$ for (c) number of clusters and (d) contribution to total rainfall. Points marked with an x show values that could not be drawn with a continuous line because adjacent bins have values that fall below 0.01%.

simulations compared to their parametrized-convection simulation. The peak in mean equivalent radius for SEVIRI was found to be ~35 km with 0.01% of storms having a mean equivalent radius of ~110 km. This is a little smaller than that found from the 8-year climatology of Sahelian $T_B$ of Mathon and Laurent (2001) who found a peak at ~40 km and 0.01% of storms at 300 km. In this study, 90% of SEVIRI clusters have an equivalent radius less than 126 km and 90% of CMORPH clusters have an equivalent radius less than ~69 km. This is larger than the <40-km equivalent radius found for 90% of sub-Saharan MCS cloud clusters determined from a single season of 85-GHz ice scattering data (Mohr et al., 1999).

In summary, with the exception of I_P25, simulated storms are too small compared to observations, and the largest simulated storms contribute too little to rainfall. The V_CP4 and V_CP12 simulations show some improvement in size distributions over the V_P12 simulation.

### 4.5. Intensity

In this section simulations are assessed for how well they represent the distribution of storm rainfall intensities. The distributions of the maximum of the cluster-mean rain rate reached during the lifetime of MCS storms is shown in Figure 5a. V_CP4 and V_CP12 show very similar distributions with a broad peak from 5 to 18 mm/hr. The distribution for CMORPH is much narrower and more similar to that for parameterized-convection simulations (V_P12 and I_P25), peaking around 5 mm/hr. Maximum intensity in I_CP4 peaks around 5 mm/hr, but the distribution has a very long tail reaching to 140 mm/hr; this occurs despite the inclusion of conservation of moisture, which has reduced very high precipitation rates in I_CP4 (see Stratton et al., 2018). Parameterized-convection simulations (V_P12 and I_P25) also more closely match CMORPH in the cluster distribution of mean intensities in terms of cluster number and contribution to total rainfall (Figures 5b and 5c), with V_CP4, V_CP12, and I_CP4 having too high mean intensities. Figures 5b
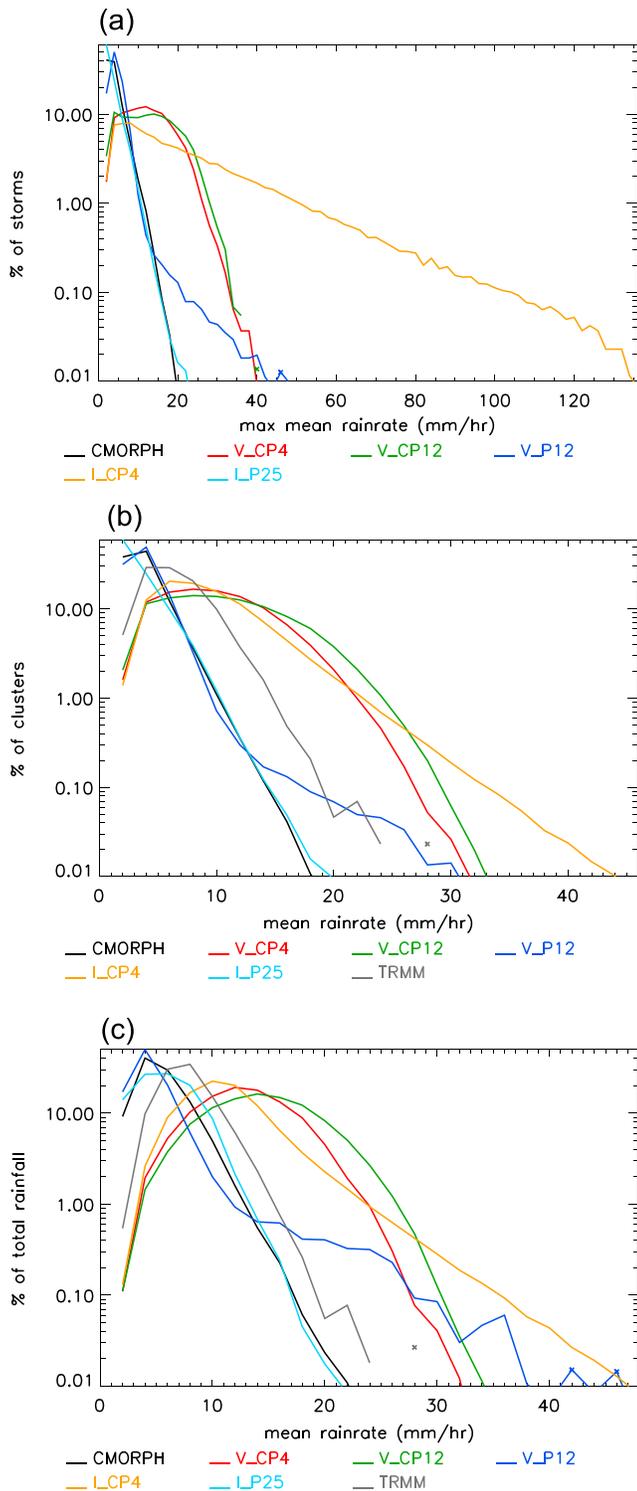
**Figure 5.** (a) Maximum storm intensity distributions for MCS over land, binned every 2 mm/hr, and intensity distributions binned every 2 mm/hr for (b) number of clusters and (c) contribution to total rainfall. Points marked with an x show values that could not be drawn with a continuous line because adjacent bins have values that fall below 0.01%.

and 5c also include data from the TRMM radar. The TRMM radar data have slightly higher intensities than CMORPH (peak shifting from 4 mm/hr for CMORPH to 6–7 mm/hr for TRMM), suggesting that CMORPH may underestimate intensity, but the TRMM intensity is still not as high as that in convection-permitting simulations. It should be noted that the I_P25 simulation used hourly mean precipitation, which one would expect to have lower values than 15-min mean or instantaneous values.

In summary, the convection-permitting simulations are producing rain events that are too intense and parameterized-convection simulations better match the rain rate intensity distributions. Although convection-permitting simulations better represent cloud top temperature distributions compared to parameterized-convection simulations (see supporting information Figure S6), their coldest cloud shields are not quite cold enough (~5 K too warm).

### 4.6. Propagation

In this section simulations are assessed for how well they represent the propagation of storms, in terms of speed and direction. Convective cloud clusters have previously been found to propagate westward over the Sahel at 8–12 m/s (Mathon & Laurent, 2001). Mean propagation speed was determined from distance traveled over the whole life of the storm divided by its lifetime. The distance traveled was determined from the center of the storm at the end of life and start of life. The peak in mean propagation speed for MCSs in convection-permitting simulations (V_CP4, V_CP12, and I_CP4) is about 4 m/s, whereas in CMORPH it is about 8 m/s (Figure 6a). Propagation speeds in parameterized-convection simulations (V_P12 and I_P25) are more scattered, because storms are often not really propagating but appear for one time step and are replaced by a new storm at a neighboring location, which the algorithm interprets as an effective propagation. A large percentage of storms in I_P25 have zero speed. MCSs tend to propagate in a westward direction in CMORPH, V_CP4, V_CP12, and I_CP4, whereas for V_P12 and I_P25 there is no preferred direction of propagation (Figure 6b). For storms tracked using SEVIRI $T_B$ the peak propagation speed (7–8 m/s) was found to be at the lower end of that found by Mathon & Laurent, (2001) for Sahelian storms (see supporting information Figure S7). Convection-permitting simulations were found to match SEVIRI well in terms of propagation of cold cloud features unlike parameterized-convection simulations. Reinarez Martínez and Chaboureau (2018) also found improvements in the propagation of brightness-temperature-tracked storms over West Africa in their convection-permitting simulations compared to their parametrized-convection simulation.

In summary, convection-permitting simulations propagate their cold cloud features at a similar rate and direction to observations, consistent with the model generating organized convective dynamics with some resemblance to reality. However, the convection-permitting simulations propagate their precipitation features about half the speed of observed precipitation features. In contrast, propagation is very poorly handled in the parameterized-convection simulations, which do not propagate their precipitation features in a westward preferred direction, since their convective activity is not coherently organized.
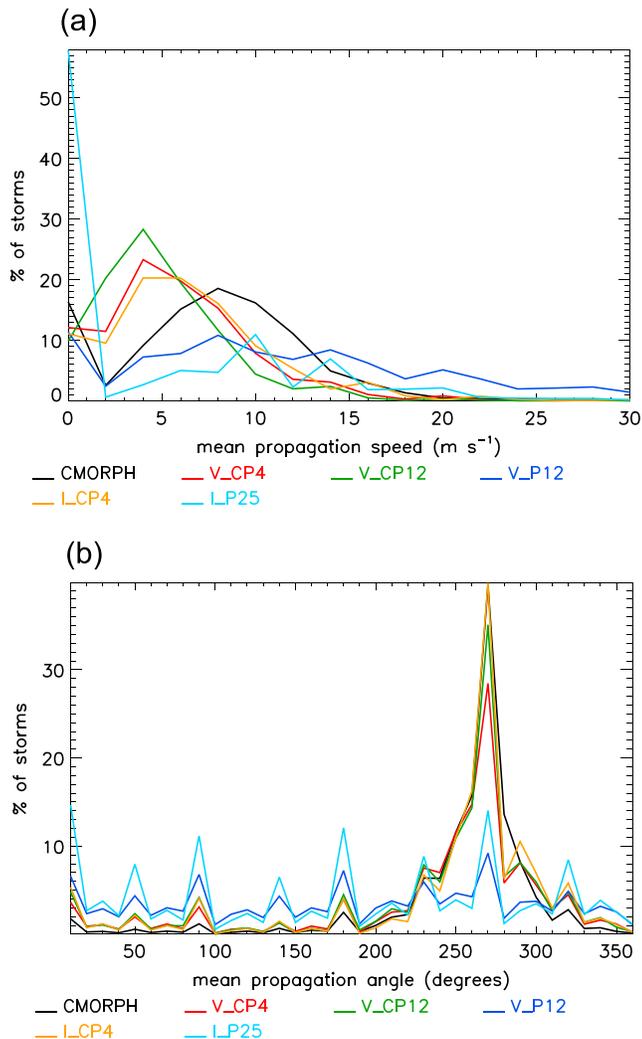
(a)



(b)



**Figure 6.** (a) Mean propagation speed distributions binned every 1 m/s and (b) mean propagation direction distributions binned in 10° angles for MCS over land.

### 4.7. Spatial Distribution of Different MCS Types

Different MCS types (e.g., fast or slow moving; short or long lived) have different climatological distributions across West Africa according to the prevailing thermodynamic conditions and wind profiles. Their distributions are important to the climatological patterns of rainfall across the continent and to the response of the rainfall to synoptic controls, for instance, propagation of storms downstream of preferred initiation zones such as mountains can be critical to water resources of those downstream regions.

Studies using tracking of Meteosat infrared brightness temperatures in West Africa have found that long-lived (>24 hr) MCSs tend to initiate farther north than shorter-lived MCSs and the fastest-moving MCSs tend to initiate in the central Sahel around 12°N (Mathon & Laurent, 2001). Bennartz and Schroeder (2011) showed that although most MCSs initiate south of the climatological African Easterly Jet (AEJ), there is a south to north gradient in lifetime and speed with the longest-living and fastest-moving MCSs tending to initiate close to or even north of the AEJ. Lafore et al. (2017) examined the locations of MCSs classified into four different types—short-lived slow storms (C1), long-lived slow storms (C2), short-lived fast storms (C3), and long-lived fast storms (C4) and also found that these C4 MCS tend to occur further inland than other types. In this study, the locations of different types of storms were assessed using these same C1 to C4 classifications. Short-lived storms are defined here as having a lifetime of <9 hr to distinguish between those storms that do/do not persist through the night, and slow storms are defined here as having a propagation speed of <8 m/s. Note that this speed threshold is lower than that in Lafore et al. (2017) (10 m/s) because propagation speeds determined in this study are somewhat lower than previously found (see section 4f). Spatial distribution maps for the four JJA seasons for CMORPH, I_CP4, and I_P25 are shown in Figures 7 (track density defined as the count of all events in each grid box normalized by the number of months analyzed and the time step used in tracking) and 8 (rainfall contribution by type defined as the rainfall accumulation from the MCS type divided by the total rainfall accumulation for all MCS types in a grid box). Spatial distribution maps for June–July 2014 for CMORPH, V_CP4, V_CP12, and V_P12 are in supporting information Figures S8 and S9.

The position of the AEJ shown by crosses in these figures was determined from the meridional maximum in the 650-hPa easterly wind (simulated in the given model or taken from ERA-Interim for the observed storms).

Considering the distribution of storms across classes, C1 storms are the most frequent type (~60%), and C4 storms are the least frequent type (3%) for CMORPH as has been previously found in observations (Lafore et al., 2017). This is also true for all simulations (~70% C1, up to 1% C4) except V_P12, which has 38% C1 storms and 61% C3. The propagation speeds in V_P12 can be quite large even though this model does not generate clearly organized convective objects but has contiguous areas of independently precipitating grid cells (see section 4 g). C3 is the second most frequent type (~32%) for CMORPH and for V_CP4, I_CP4, and I_P25; However, V_CP12 has more C2 storms. This is because V_CP12 has storm lifetimes that tend to be longer than CMORPH and other simulations and propagation speeds that are slower than CMORPH. Parameterized-convection simulations (V_P12 and I_P25) have more C3 storms (61% and 29%, respectively) compared to convection-permitting simulations (9%–19%) because lifetimes of storms in V_P12 and I_P25 are lower.

The spatial distributions of the track densities of different MCS types are now assessed (see Figures 7 and S8). In CMORPH, spatial distributions tend to be slightly further north in Figure 7 than in Figure S8 because
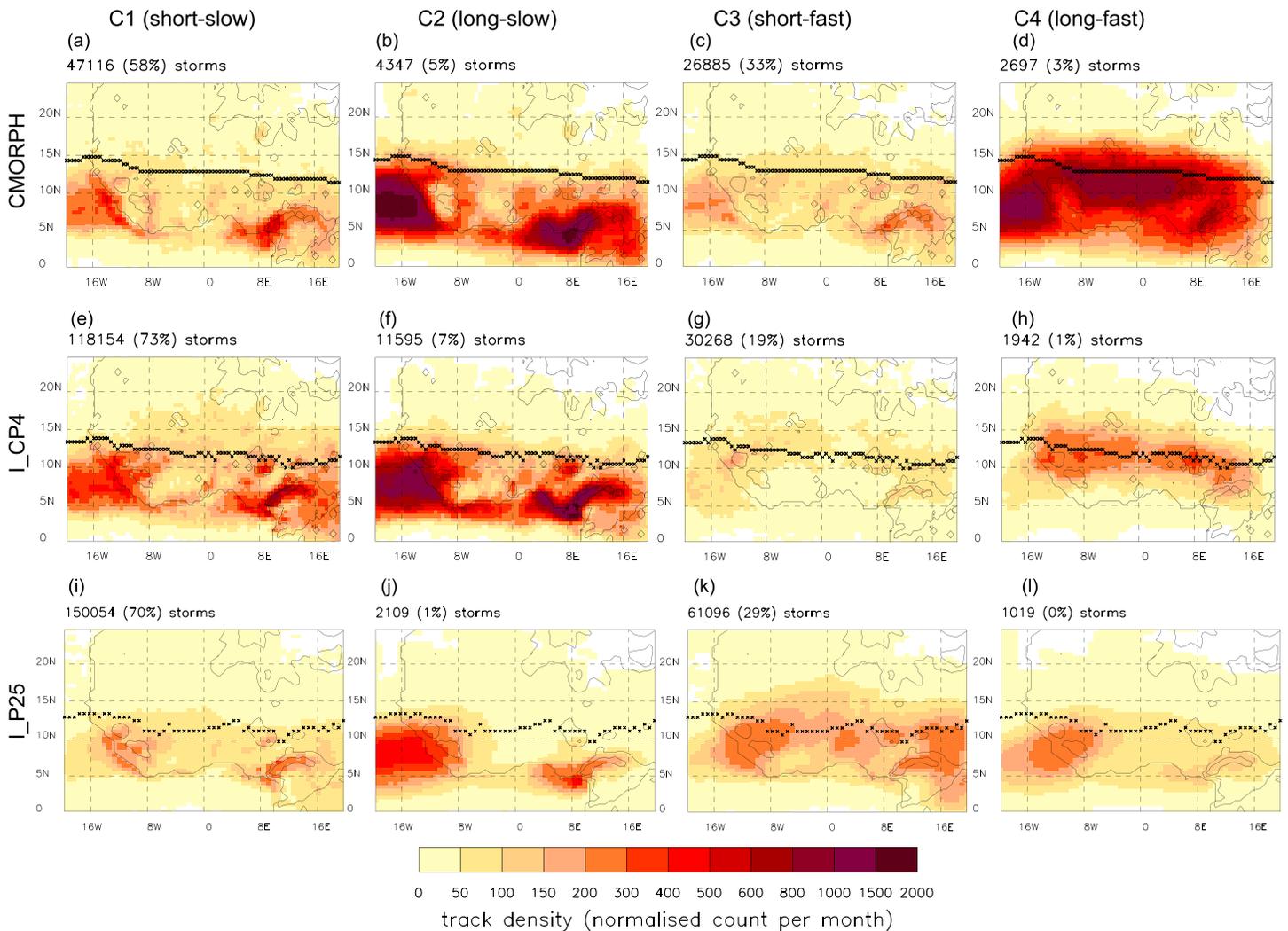
**Figure 7.** Maps showing MCS storm track densities over all four years for (a to d) CMORPH, (e to h) I_CP4, and (i to l) I_P25 for the different types of MCS storms (from left to right C1, C2, C3, and C4). Orography is shown as a gray contour at the 500-m level. The position of the AEJ is shown as black crosses. All plots regridded to ~50-km grid.

August is also included and the AEJ is also slightly further north. The long-lived storms (C2 and C4) have higher track densities than the short-lived storms (C1 and C3) in CMORPH because of their longer lifetime but also because they have larger mean areas (Table 3). This is also true of convection-permitting simulations but not so for the parameterized-convection simulations, which have a much greater proportion of short-lived storms despite their long-lived storms having considerably larger areas than their short-lived storms.

In CMORPH, C1 storms occur mostly around the coast, in the ocean south of 10°N and west of 10°W, and over high land such as the Cameroon Mountains (10°E, 6°N); C2 storms occur even more predominantly around the coast, in the ocean south of 10°N and west of 10°W, and the Cameroon Mountains; C3 storms have lower track densities in the ocean and around the coast, and higher track densities over high land and close to the AEJ; C4 storms have track densities clearly shifted inland closer to the AEJ. The track densities for convection-permitting simulations, particularly I_CP4, match these spatial distributions better than those of parameterized-convection simulations. In particular, north of the AEJ the parameterized-convection simulations tend to be dominated by C3 storms (due to their short storm lifetimes), while the observations are dominated by C4 storms and convection-permitting simulations by C1, C2, and C4 storms. The convection-permitting simulations have more C1 and C2 storms north of the AEJ due to their storm
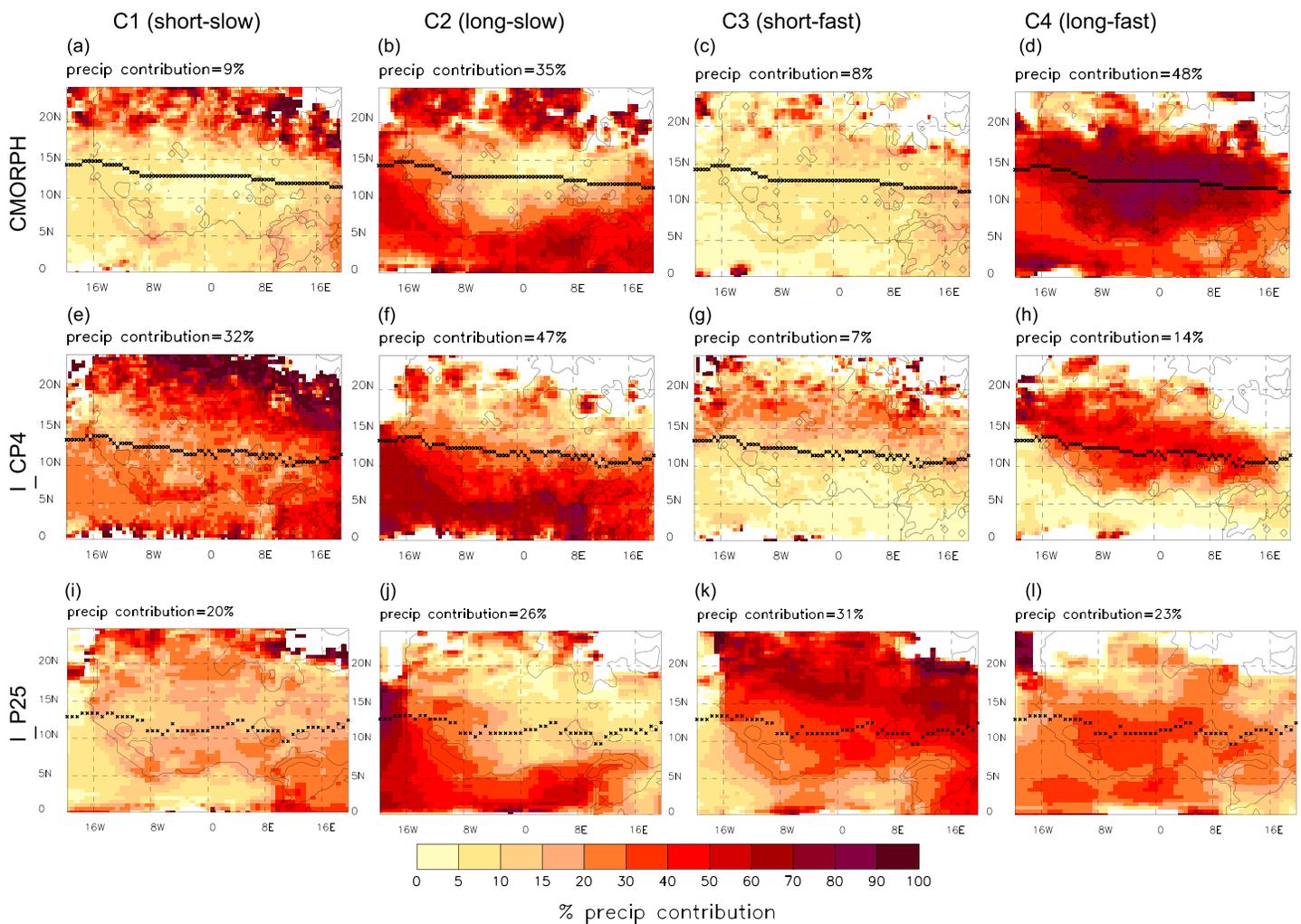
**Figure 8.** Maps showing contributions to rainfall accumulation over all 4 years for (a to d) CMORPH, (e to h) I_CP4, and (i to l) I_P25 from the different types of MCS storms (from left to right C1, C2, C3, and C4). Orography is shown as a gray contour at the 500-m level. The position of the AEJ is shown as black crosses. All plots regridded to ~50-km grid.

**Table 3**
*Mean Areas and Rain Rates of Different Types of MCS*

|  |  | C1 | C2 | C3 | C4 |
|---|---|---|---|---|---|
| Mean area (km$^2$) or relative mean area to C1 type | CMORPH | 2,452 | ×4.9 | ×1.2 | ×7.9 |
|  | V_CP4 | 1,537 | ×2.3 | ×1.2 | ×3.9 |
|  | V_CP12 | 1,780 | ×2.3 | ×1.1 | ×3.5 |
|  | V_P12 | 1,390 | ×9.3 | ×1.3 | ×70.9 |
|  | I_CP4 | 1,366 | ×2.7 | ×1.3 | ×5.1 |
|  | I_P25 | 2,431 | ×8.0 | ×2.3 | ×15.4 |
| Mean rain rate (mm/hr) or relative mean rain rate to C1 type | CMORPH | 2.04 | ×1.4 | ×1.0 | ×1.6 |
|  | V_CP4 | 6.61 | ×1.1 | ×0.9 | ×1.4 |
|  | V_CP12 | 6.51 | ×1.3 | ×0.7 | ×1.4 |
|  | V_P12 | 2.92 | ×0.9 | ×1.1 | ×0.8 |
|  | I_CP4 | 10.26 | ×1.1 | ×0.7 | ×0.9 |
|  | I_P25 | 1.89 | ×1.6 | ×1.1 | ×2.1 |

propagation speeds being too slow compared to CMORPH. Arguably, I_CP4 has the best representation of the observed dominance of C4 storms north of the AEJ. Overall, the spatial distributions for parameterized-convection simulations do not vary substantially from MCS type to type, relative to the observations and convection-permitting simulations.

The spatial distributions of contribution to precipitation accumulations of different MCS types are now assessed (see Figures 8 and S9). In CMORPH, the spatial distributions are similar to the track density distributions, with the C2 storms contributing largely to coastal precipitation and C4 storms contributing largely to inland precipitation close to and north of the AEJ: most of the CMORPH precipitation comes from long-lived systems. All of the convection-permitting simulations have a good representation of these C2 and C4 contributions and spatial distributions. However, they also tend to have too much rain from C1 (short-lived and slow-moving) storms. There is low skill in capturing the spatial patterns of the observed precipitation contributions in parameterized-convection simulations.

Although C4 storms are the least frequent in number, they contribute almost 50% of the MCS precipitation in CMORPH (consistent with the high cloud coverage of long-lived systems in Mathon and Laurent, 2001). One would expect a long-lived storm to contribute more to the precipitation than a short-lived storm simply because it is raining for longer, but the mean storm area of long-lived storms is also considerably larger than that of short-lived storms (Table 3). This difference in mean area and lifetime explains a large part of the different precipitation contributions in CMORPH and all simulations. Long-lived storms also have slightly higher mean rainfall intensities than short-lived storms for CMORPH and all simulations except for V_P12 where the reverse is true.

In summary, parameterized-convection simulations have more uniform spatial distributions of all the evaluated storm types compared to CMORPH and convection-permitting simulations; that is, the type of MCS is less dependent on location for parameterized-convection simulations. C4 storms in CMORPH and convection-permitting simulations occur more inland and closer to the AEJ than other types of storm. The AEJ in parameterized-convection simulations is in a similar location to that in the convection-permitting simulations, suggesting that the AEJ (and associated thermodynamic patterns; Parker et al., 2005) is having less impact on lifetime or speed of storms in parameterized-convection simulations than in the convection-permitting simulations or in reality. C4 storms in CMORPH and all simulations are the least frequent type but have the largest mean area. That, combined with longer lifetimes than the C1 and C3 storms, means that they can contribute considerably to total rainfall over the whole region, although this contribution is greater in CMORPH than in simulations. The prevalence of the long-lived C2 and C4 storms in observations and in the convection-permitting simulations is a key factor in the impact of the rainfall, for instance, in the distributions of rainfall downstream of preferred triggering regions, or in the accumulation of rainfall at one geographical location.

## 5. Discussion and Conclusions

A storm-tracking algorithm described in section 3 was used to generate storm-centered statistics based on rainfall and OLR/brightness temperature data from convection-permitting simulations, parameterized-convection simulations, and observations. These statistics were compared between the different simulations and observations. Where possible, these statistics have also been compared to previously determined statistics and found to agree well.

The numbers, percentages of MCSs, and contributions to rainfall from MCSs are generally more realistic in convection-permitting simulations than parameterized-convection simulations. The spatial distribution of different classifications of MCSs is also more realistic in convection-permitting simulations than parameterized-convection simulations.

The diurnal cycle of MCS initiations and dissipations is improved in convection-permitting simulations for rainfall. The improvement in the timing of initiations is small between I_P25 and I_CP4 (UM10.3 model) compared to that between V_P12 and V_CP12 (older UM8.2 model), because initiations happen later in I_P25 compared to V_P12 and earlier in I_CP4 compared to V_CP4. This is likely due to the added stochastic perturbations in the boundary layer in UM10.3 and the different spatial resolution of the I_P25 simulation. Storm lifetimes are improved in convection-permitting simulations with parameterized-convection simulations having too short lifetimes compared to observations.

In terms of size and intensity, MCSs develop more slowly in convection-permitting simulations than in parameterized-convection simulations. Parameterized-convection simulations develop too quickly compared to observations.

With the exception of I_P25, simulated storms are too small compared to observations and the largest simulated storms contribute too little to rainfall. The V_CP4 and V_CP12 simulations show some improvement in size distributions over the V_P12 simulation.

The rain rate of storms is not improved in convection-permitting simulations. In fact, convection-permitting simulations have too high intensity, and this has not improved much in the UM10.3 model (I_CP4) compared to the older UM8.2 model (V_CP4/12), and the parameterized-convection simulations match better with CMORPH. Although the JJA seasonal mean precipitation in I_CP4 looks closer to GPCP observations than that in I_P25 (Stratton et al., 2018), the seasonal mean rainfall accumulations over the land area were

found to be greater for the convection-permitting simulations than parameterized-convection simulations and for all simulations compared to CMORPH. For I_CP4 and I_P25 the spatial biases for June through August were very similar to those found by Berthou et al. (2019) for July through September showing a large overestimate of rainfall in the Guinea Highlands. The V_CP4, V_CP12, and V_P12 simulations also showed this same bias but with positive bias over more of the land area for V_CP4 and V_CP12 (not shown). All simulations still have a positive bias even if low land areas only are compared showing the bias is not just restricted to the Guinea Highlands. It is likely that both CMORPH and TRMM radar underestimate the highest rain rates and this modeled storm intensity bias would not be as bad as these results suggest if comparisons against rain gauge data could be used. This high rain rate is likely due to underresolved updraughts and insufficient turbulent mixing at 4-km resolution (Kendon et al., 2012). Modeled OLR distributions compared to SEVIRI brightness temperature distributions are considerably improved in convection-permitting simulations, although the models do not achieve the coldest cloud shields.

Different subgrid turbulence schemes (Machado & Chaboureau, 2015; Pearson et al., 2014) have been shown to affect the size of cold cloud clusters and rainfall clusters, not only in terms of whether 1-D or 3-D schemes are used but also the mixing length used. Although the convection-permitting simulations in this study use the better 3-D scheme, the mixing length has not been optimized to produce storms of the correct size and intensity. The ability to accurately simulate MCS has also been shown to be dependent on the cloud microphysical parameterization (Van Weverberg et al., 2013). Microphysics schemes that allow buildup of ice aloft lead to larger or more numerous MCSs with larger anvils. I_CP4 uses the same cloud microphysics scheme as I_P25, yet I_CP4 and I_P25 have very different storm sizes. I_CP4 also has 3-D Smagorinsky subgrid turbulence and convection switched off leading to more intense and smaller storms. The older VERA simulations have a simpler microphysics scheme, but the size distributions of cold cloud are not discernibly different for V_CP4 and I_CP4, although I_CP4 rainfall-tracked storms are generally smaller than V_CP4.

Storms in parameterized-convection simulations do not propagate coherently. Many have zero speed although some storms have speeds of up to 30 m/s or more, and they show no preferred direction of propagation. This feature is essentially because many instances of *propagation* in the parametrized storms are actually cases where storms are very short lived and are initiated and decay close to each other with little dynamical coupling. It is almost impossible for the tracking algorithm to distinguish between truly coherent, propagating storms and those which are in proximity, but uncoupled dynamically. However, the lack of preferred propagation direction (Figure 6b) indicates that the parametrized storms are most commonly lacking a dynamical control.

Storms in convection-permitting simulations do propagate in a westward direction like observed storms but do not propagate fast enough (4 m/s compared to 8 m/s) when tracking is performed with rainfall. However, when storms are tracked using OLR in convection-permitting simulations, the propagation speed matches closely to observations. This shows that in convection-permitting simulations, convective activity is more coherently organized and therefore, even at 12-km resolution it is preferable to disable the convection parameterization.

Overall, convection-permitting simulations show improvements over parameterized-convection simulations of several metrics of storms based on precipitation tracking (improvements were less for OLR tracking). These metrics tend to be those which are particularly important in studies of the impacts of tropical rainfall, including the lifetimes or storms and their speeds and spatial distributions relative to the topography. However, convection-permitting simulations tend to propagate their rain features too slowly and rain too intensely over too small an area, and caution must still be employed when applying these models even though they are preferable to running with the convection parameterization enabled. Further analysis of the simulations in this study is being carried out to better understand the thermodynamic and dynamic drivers of the development of these modeled storms.

## References

Baldauf, M., Seifert, A., Förstner, J., Majewski, D., Raschendorfer, M., & Reinhardt, T. (2011). Operational convective-scale numerical weather prediction with the COSMO model: Description and sensitivities. *Monthly Weather Review*, *139*(12), 3887–3905. https://doi.org/10.1175/MWR-D-10-05013.1

Ban, N., Schmidli, J., & Schär, C. (2015). Heavy precipitation in a changing climate: Does short-term summer precipitation increase faster? *Geophysical Research Letters*, *42*, 1165–1172. https://doi.org/10.1002/2014GL062588

Bennartz, R., & Schroeder, M. (2011). Convective activity over Africa and the tropical Atlantic inferred from 20 years of geostationary Meteosat infrared observations. *Journal of Climate*, *25*(1), 156–169. https://doi.org/10.1175/2011JCLI3984.1

Berthou, S., Rowell, D. P., Kendon, E. J., Roberts, M., Stratton, R., Crook, J., & Wilcox, C. (2019). Improved climatological precipitation characteristics over West Africa at convection-permitting scales. *Climate Dynamics*. https://doi.org/10.1007/s00382-019-04759-4

Best, M. J., Pryor, M., Clark, D. B., Rooney, G. G., Essery, R. L. H., M'enard, C. B., et al. (2011). The Joint UK Land Environment Simulator (JULES), model description - Part 1: Energy and water fluxes. *Geoscientific Model Development*, *4*, 677–699. https://doi.org/10.5194/gmd-4-701-2011

Birch, C. E., Parker, D. J., Marsham, J. H., Garcia-Carreras, L., & Copsey, D. (2014). A seamless assessment of the role of convection in the water cycle of the West African Monsoon. *Journal of Geophysical Research: Atmospheres*, *119*, 2890–2912. https://doi.org/10.1002/2013JD020887

Birch, C. E., Parker, D. J., O'Leary, A., Marsham, J. H., Taylor, C. M., Harris, P., & Lister, G. (2013). Impact of soil moisture and convectively generated waves on the initiation of a West African mesoscale convective system. *Quarterly Journal of the Royal Meteorological Society*, *139*(676), 1712–1730. https://doi.org/10.1002/qj.2062

Caine, S., Lane, T. P., May, P. T., Jakob, C., Siems, S. T., Manton, M. J., & Pinto, J. (2013). Statistical assessment of tropical convection-permitting model simulations using a cell-tracking algorithm. *Monthly Weather Review*, *141*(2), 557–581. https://doi.org/10.1175/MWR-D-11-00274.1

Clark, A. J., Bullock, R. G., Jensen, T. L., Xue, M., & Kong, F. (2014). Application of object-basedtime-domain diagnostics for tracking precipitation systems in convection-allowing models. *Weather and Forecasting*, *29*(3), 517–542. https://doi.org/10.1175/WAF-D-13-00098.1

Clark, D. B., Mercado, L. M., Sitch, S., Jones, C. D., Gedney, N., Best, M. J., et al. (2011). The Joint UK Land Environment Simulator (JULES), model description—Part 2: Carbon fluxes and vegetation dynamics. *Geoscientific Model Development*, *4*(3), 701–722. https://doi.org/10.5194/gmd-4-701-2011

Clark, P., Roberts, N., Lean, H., Ballard, S. P., & Charlton-Perez, C. (2016). Convection-permitting models: A step-change in rainfall forecasting. *Meteorological Applications*, *23*(2), 165–181. https://doi.org/10.1002/met.1538

Davies, T., Cullen, M. J. P., Malcolm, A. J., Mawson, M. H., Staniforth, A., White, A. A., & Wood, N. (2005). A new dynamical core for the Met Office's global and regional modelling of the atmosphere. *Quarterly Journal of the Royal Meteorological Society*, *131*(608), 1759–1782. https://doi.org/10.1256/qj.04.101

Dee, D. P., Uppala, S. M., Simmons, A. J., Berrisford, P., Poli, P., Kobayashi, S., et al. (2011). The ERA-Interim reanalysis: Configuration and performance of the data assimilation system. *Quarterly Journal of the Royal Meteorological Society*, *137*(656), 553–597. https://doi.org/10.1002/qj.828

Futyan, J. M., & Del Genio, A. D. (2007). Deep convective system evolution over Africa and the tropical Atlantic. *Journal of Climate*, *20*(20), 5041–5060. https://doi.org/10.1175/JCLI4297.1

Garcia-Carreras, L., Challinor, A. J., Parkes, B. J., Birch, C. E., Nicklin, K. J., & Parker, D. J. (2015). The impact of parameterized convection on the simulation of crop processes. *Journal of Applied Meteorology and Climatology*, *54*(6), 1283–1296. https://doi.org/10.1175/JAMC-D-14-0226.1

Garcia-Carreras, L., Marsham, J. H., Parker, D. J., Bain, C. L., Milton, S., Saci, A., et al. (2013). The impact of convective cold pool outflows on model biases in the Sahara. *Geophysical Research Letters*, *40*, 1647–1652. https://doi.org/10.1002/grl.50239

Goyens, C., Lauwaet, D., Schroder, M., Demuzere, M., & Van Lipzig, N. P. M. (2011). Tracking mesoscale convective systems in the Sahel: Relation between cloud parameters and precipitation. *International Journal of Climatology*, *32*(12), 1921–1934. https://doi.org/10.1002/joc.2407

Gregory, D., & Rowntree, P. R. (1990). A mass-flux convection scheme with representation of cloud ensemble characteristics and stability-dependent closure. *Monthly Weather Review*, *118*(7), 1483–1506. https://doi.org/10.1175/1520-0493(1990)118<1483:AMFCSW>2.0.CO;2

Hartley, A. J., Parker, D. J., Garcia-Carreras, L., & Webster, S. (2016). Simulation of vegetation feedbacks on local and regional scale precipitation in West Africa. *Agricultural and Forest Meteorology*, *222*, 59–70. https://doi.org/10.1016/j.agrformet.2016.03.001

Joyce, R. J., Janowaik, J. E., Arkin, P. A., & Xie, P. (2004). CMORPH: A method that produces global precipitation estimates from passive microwave and infrared data at high spatial and temporal resolution. *Journal of Hydrometeorology*, *5*(3), 487–503. https://doi.org/10.1175/1525-7541(2004)005<0487:CAMTPG>2.0.CO;2

Kendon, E. J., Ban, N., Roberts, N. M., Fowler, H. J., Roberts, M. J., Chan, S. C., et al. (2017). Do convection-permitting regional climate models improve projections of future precipitation change?*Bulletin of the American Meteorological Society*, *98*(1), 79–93. https://doi.org/10.1175/BAMS-D-15-0004.1

Kendon, E. J., Roberts, N. M., Senior, C. A., & Roberts, M. J. (2012). Realism of rainfall in a very high-resolution regional climate model. *Journal of Climate*, *25*(17), 5791–5806. https://doi.org/10.1175/JCLI-D-11-00562.1

Kirtsetter, P.-E., Hong, Y., Gourley, J. J., Schwaller, M., Peterson, W., & Zhang, J. (2013). Comparison of TRMM 2A25 products, version 6 and version 7, with NOAA/NSSL ground radar–based National Mosaic QPE. *Journal of Hydrometeorology*, *14*(2), 661–669. https://doi.org/10.1175/JHM-D-12-030.1

Klein, C., Bliefernicht, J., Heinzeller, D., Gessner, U., Klein, I., & Kuntsmann, H. (2017). Feedback of observed interannual vegetation change: A regional climate model analysis for the West African monsoon. *Climate Dynamics*, *48*(9-10), 2837–2858. https://doi.org/10.1007/s00382-016-3237-x

Lafore, J. P., Chapelon, N., Diop, M., Gueye, B., Largeron, Y., Lepape, S., et al. (2017). Deep convection. In D. J. Parker, & M. Diop-Kane (Eds.), *Meteorology of tropical West Africa: The forecasters' handbook*, (pp. 90–129). John Wiley & Sons, Ltd. https://doi.org/10.1002/9781118391297.ch3

Lean, H. W., Clark, P. A., Dixon, M., Roberts, N. M., Fitch, A., Forbes, R., & Halliwell, C. (2008). Characteristics of high resolution versions of the Met Office Unified Model for forecasting convection over the United Kingdom. *Monthly Weather Review*, *136*(9), 3408–3424. https://doi.org/10.1175/2008MWR2332.1

Lock, A. P., Brown, A. R., Bush, M. R., Martin, G. M., & Smith, R. N. B. (2000). A new boundary layer mixing scheme. Part I: Scheme description and single-column model tests. *Monthly Weather Review*, *128*(9), 3187–3199. https://doi.org/10.1175/1520-0493(2000)128<3187:ANBLMS>2.0.CO;2

Machado, L. A. T., & Chaboureau, J.-P. (2015). Effect of turbulence parameterization on assessment of cloud organization. *Monthly Weather Review*, *143*(8), 3246–3262. https://doi.org/10.1175/MWR-D-14-00393.1

Machado, L. A. T., Rossow, W. B., Guedes, R. L., & Walker, A. W. (1998). Life cycle variations of mesoscale convective systems over the Americas. *Monthly Weather Review*, *126*(6), 1630–1654. https://doi.org/10.1175/1520-0493(1998)126<1630:LCVOMC>2.0.CO;2

Marsham, J. H., Dixon, N., Garcia-Carreras, L., Lister, G., Parker, D. J., Knippertz, P., & Birch, C. (2013). The role of moist convection in the West African monsoon system-insights from continental-scaleconvection-permitting simulations. *Geophysical Research Letters*, *40*, 1843–1849. https://doi.org/10.1002/grl.50347

Mathon, V., & Laurent, H. (2001). Life cycle of Sahelian mesoscale convective cloud systems. *Quarterly Journal of the Royal Meteorological Society*, *127*(572), 377–406. https://doi.org/10.1002/qj.49712757208

Mathon, V., Laurent, H., & Lebel, T. (2002). Mesoscale Convective System Rainfall in the Sahel. *Journal of Applied Meteorology*, *41*, 1081–1092.

Maurer, V., Bischoff-Gauß, I., Kalthoff, N., Gantner, L., Roca, R., & Panitz, H. J. (2017). Initiation of deep convection in the Sahel in a convection-permitting climate simulation for northern Africa. *Quarterly Journal of the Royal Meteorological Society*, *143*(703), 806–816. https://doi.org/10.1002/qj.2966

McBeath, K., Field, P. R., & Cotton, R. J. (2014). Using operational weather radar to assess high-resolution numerical weather prediction over the British Isles for a cold air outbreak case study. *uarterly Journal of the Royal Meteorological Society*, *140*(678), 225–239. https://doi.org/10.1002/qj.2123

Mohr, K. I. (2004). Interannual, monthly, and regional variability in the wet season diurnal cycle of precipitation in sub-SaharanAfrica. *Journal of Climate*, *17*(12), 2441–2453. https://doi.org/10.1175/1520-0442(2004)017<2441:IMARVI>2.0.CO;2

Mohr, K. I., Famiglietti, J. S., & Zipser, E. J. (1999). The contribution to tropical rainfall with respect to convective system type, size, and intensity estimated from the 85-GHzice-scattering signature. *Journal of Applied Meteorology*, *38*(5), 596–606. https://doi.org/10.1175/1520-0450(1999)038<0596:TCTTRW>2.0.CO;2

Ogawa, K., & Schmugge, T. (2004). Mapping surface broadband emissivity of the Sahara Desert using ASTER and MODIS data. *Earth Interactions*, *8*(7), 1–14. https://doi.org/10.1175/1087-3562(2004)008<0001:MSBEOT>2.0.CO;2

Parker, D. J., &Diop-Kane, M. (2017). *Meteorology of tropical West Africa: The forecasters' handbook*. Wiley-Blackwell. https://doi.org/10.1002/9781118391297

Parker, D. J., Thorncroft, C. D., Burton, R. R., & Diongue-Niang, A. (2005). Analysis of the African easterly jet, using aircraft observations from the JET2000 experiment. *Quarterly Journal of the Royal Meteorological Society*, *131*(608), 1461–1482.

Pearson, K. J., Lister, G. M. S., Birch, C. E., Allan, R. P., Hogan, R. J., & Woolnough, S. J. (2014). Modelling the diurnal cycle of tropical convection across the "grey zone". *Quarterly Journal of the Royal Meteorological Society*, *140*(679), 491–499. https://doi.org/10.1002/qj.2145

Poulter, B., MacBean, N., Hartley, A., Khlystova, I., Arino, O., Betts, R., et al. (2015). Plant functional type classification for earth system models: Results from the European Space Agency's land cover climate change initiative. *Geoscientific Model Development*, *8*(7), 2315–352328. https://doi.org/10.5194/gmd-8-2315-2015

Prein, A. F., Langhans, W., Fosser, G., Ferrone, A., Ban, N., Goergen, K., et al. (2015). A review on regional convection-permitting climate modeling: Demonstrations, prospects, and challenges. *Reviews of Geophysics*, *53*, 323–361. https://doi.org/10.1002/2014RG000475

Reinares Martínez, I., & Chaboureau, J.-P. (2018). Precipitation and mesoscale convective systems: Explicit versus parameterised convection over Northern Africa. *Monthly Weather Review*, *146*(3), 797–812. https://doi.org/10.1175/MWR-D-17-0202.1

Schmetz, J., Pili, P., Tjemkes, S., Just, D., Kerkmann, J., Rota, S., & Ratier, A. (2002). An introduction to Meteosat Second Generation (MSG). *Bulletin of the American Meteorological Society*, *83*(7), 992–992. https://doi.org/10.1175/1520-0477(2002)083,0977:AITMSG.2.3.CO;2

Stein, T. H. M., Hogan, R. J., Hanley, K. E., Nicol, J. C., Lean, H. W., Plant, R. S., et al. (2014). The three-dimensional morphology of simulated and observed convective storms over Southern England. *Monthly Weather Review*, *142*(9), 3264–3283. https://doi.org/10.1175/MWR-D-13-00372.1

Stein, T. R., Hogan, R. J., Clark, P. A., Halliwell, C. E., Hanley, K. E., Lean, H. W., et al. (2015). The DYMECS project: A statistical approach for the evaluation of convective storms in high-resolution NWP models. *Bulletin of the American Meteorological Society*, *96*(6), 939–951. https://doi.org/10.1175/BAMS-D-13-00279.1

Stratton, R. A., Senior, C. A., Vosper, S. B., Folwell, S. S., Boutle, I. A., Earnshaw, P. D., et al. (2018). A pan-Africaconvection-permitting regional climate simulation with the Met Office Unified Model: CP4-Africa. *Journal of Climate*, *31*(9), 3485–3508. https://doi.org/10.1175/JCLI-D-17-0503.1

Taylor, C. M., Birch, C. E., Parker, D. J., Dixon, N., Guichard, F., Nikulin, G., & Lister, G. M. S. (2013). Modeling soil moisture-precipitation feedback in the Sahel: Importance of spatial scale versus convective parameterization. *Geophysical Research Letters*, *40*, 6213–6218. https://doi.org/10.1002/2013GL058511

Van Weverberg, K., Vogelmann, A. M., Lin, W., Luke, E. P., Cialella, A., Minnis, P., et al. (2013). The role of cloud microphysics parameterization in the simulation of mesoscale convective system clouds and precipitation in the tropical Western Pacific. *Journal of the Atmospheric Sciences*, *70*(4), 1104–1128. https://doi.org/10.1175/JAS-D-12-0104.1

Vogel, R. L., Liu, Q., Han, Y., & Weng, F. (2011). Evaluating a satellite-derived global infrared land surface emissivity data set for use in radiative transfer modelling. *Journal of Geophysical Research*, *116*, D08105. https://doi.org/10.1029/2010JD014679

Weedon, G. P., Balsamo, G., Bellouin, N., Gomes, S., Best, M. J., & Viterbo, P. (2014). The WFDEI meteorological forcing data set: WATCH forcing data methodology applied to ERA-Interim reanalysis data. *Water Resources Research*, *50*, 7505–7514. https://doi.org/10.1002/2014WR015638

Weusthoff, T., Ament, F., Arpagaus, M., & Rotach, M. (2010). Assessing the benefits of convection-permitting models by neighborhood verification: Examples from MAP D-PHASE. *Monthly Weather Review*, *138*(9), 3418–3433. https://doi.org/10.1175/2010MWR3380.1

Wilson, D. R., & Ballard, S. P. (1999). A microphysically based precipitation scheme for the UK Meteorological Office Unified Model. *Quarterly Journal of the Royal Meteorological Society*, *125*(557), 1607–1636. https://doi.org/10.1002/qj.49712555707

Xie, P., Joyce, R., Wu, S., Yoo, S.-H., Yarosh, Y., Sun, F., & Lin, R. (2017). Reprocessed, bias-corrected CMORPH global high-resolution precipitation estimates from 1998. *Journal of Hydrometeorology*, *18*(6), 1617–1641. https://doi.org/10.1175/JHM-D-16-0168.1

Yang, Q., Houze, R. AJr., Leung, L. R., & Feng, Z. (2017). Environments of long-lived mesoscale convective systems over the central United States in convection permitting climate simulations. *Journal of Geophysical Research: Atmospheres*, *122*, 13,288–13,307. https://doi.org/10.1002/2017JD027033

Zhou, D. K., Larar, A. M., Liu, X., Smith, W. L., Strow, L. L., Yang, P., et al. (2011). Global land surface emissivity retrieved from satellite ultraspectral IR measurements. *IEEE Transactions on Geoscience and Remote Sensing*, *49*(4), 1277–1290. https://doi.org/10.1109/TGRS.2010.2051036